Biomaterials 57 (2015) 161–168

Contents lists available at ScienceDirect

Biomaterials

journal homepage: www.elsevier.com/locate/biomaterials

Mapping the CXCR4 receptor on breast cancer cells

Biran Wang [a], Peng Guo [a, b, c], Debra T. Auguste [a, *]

[a] Department of Biomedical Engineering, The City College of New York, 160 Convent Avenue, New York, NY 10031, United States
[b] Vascular Biology Program, Boston Children's Hospital, 300 Longwood Avenue, Boston, MA 02115, United States
[c] Department of Surgery, Harvard Medical School and Boston Children's Hospital, 300 Longwood Avenue, Boston, MA 02115, United States

ARTICLE INFO

Article history:
Received 30 September 2014
Received in revised form
3 April 2015
Accepted 8 April 2015
Available online

Keywords:
Atomic force microscopy (AFM)
CXCR4
Breast cancer
Young's modulus
Adhesion
Drug delivery

ABSTRACT

The CXCR4 receptor triggers cell migration and, in breast cancer, promotes metastasis. To date, the dynamic assembly of CXCR4 on the cell surface as a mediator of receptor binding is not well characterized. The objective of this work is to quantify the density, spatial organization, and magnitude of binding of the CXCR4 receptor on live metastatic breast cancer (MBC) cells. We measured the Young's modulus, the CXCR4 surface density, and CXCR4 unbinding force on MBC cells by atomic force microscopy. We conclude that the CXCR4 density, spatial organization, and matrix stiffness are paramount to achieve strong binding.

1. Introduction

Breast cancer remains a significant cause of death in the world, claiming 40,000 lives each year in the United States alone [1]. Once a cancer metastasizes, the 5-year patient survival rate plummets from 99% for stage I to 22% for stage IV [2]. Identification of mechanisms leading to metastasis may be critical to understanding and treating the disease.

Chemokine receptors are the major regulators of cell trafficking and adhesion; their role in cancer metastasis is under intense investigation. In particular, C-X-C chemokine receptor type 4 (CXCR-4 or CD184) has been implicated in both tumor cell dissemination from the primary site and intravasation via trans-endothelial migration [3]. The interaction of CXCR4 with its ligand stromal cell-derived factor 1 (SDF-1 or CXCL12) promotes breast cancer metastasis and angiogenesis. Although gene expression analysis shows an overexpression of CXCR4, quantification of the surface density and spatial organization of CXCR4 on breast cancer cell membranes has yet to be determined. Furthermore, the overall effect of CXCR4 organization on binding is unknown despite reports of association within lipid rafts [4].

Since its invention in the early 1980s by Binnig et al., Atomic Force Microscopy (AFM) has become widely used to characterize surface topology and mechanical properties of materials at the submicron scale [5]. AFM may be used to describe cell morphology, rheological properties and ligand/receptor interactions in aqueous environments. AFM is often reserved for single ligand/receptor interactions or homogeneous environments. The heterogeneity of the cell membrane is often not a focus.

In this study, AFM was used to characterize the density and organization of CXCR4 on the surface of four human breast cancer cell lines: two triple negative breast cancer (TNBC) cell lines (MDA-MB-231 and MDA-MB-436), one estrogen receptor (ER) positive cell line (MCF-7), and one human epidermal growth factor receptor 2 (HER2) over-expressing cell line (SKBR3). The non-neoplastic human mammary cell lines, MCF10A and AG11132, were used as controls. Herein, we identify factors that promote strong adhesion between engineered surfaces and cancer cells. This work may lead to improved engineering of targeted drug delivery vehicles.

2. Materials and methods

2.1. Cell culture

Human breast cancer cell lines were grown in a humidified atmosphere (5% CO_2) at 37 °C. Six cell lines were studied: MDA-MB-231 cells were kindly provided by Dr. Bingmei Fu's lab (City College

* Corresponding author. Grove School of Engineering, The City College of New York, 160 Convent Avenue T509, New York, NY 10031, United States. Tel.: +1 (212) 650 7165; fax: +1 (212) 650 6727.
E-mail address: dauguste@ccny.cuny.edu (D.T. Auguste).

http://dx.doi.org/10.1016/j.biomaterials.2015.04.023
0142-9612/

of The City University of New York). MCF 10A, AG11132, SKBR3, MCF-7 and MDA-MB-436 were kindly provided by Dr. Marsha Moses at Children's Hospital Boston.

MDA-MB-231 MCF-7 and MDA-MB-436 cells were cultured in DMEM (Corning, Corning, NY), supplemented with 10% FBS (Life Technologies, Carlsbad, CA) + 1% Pen/Strep (Life Technologies, Carlsbad, CA). SKBR3 cells were cultured in McCoy5a (Life Technologies, Carlsbad, CA) + 10% FBS. MCF10A cells were cultured in DMEM/F12 (Life Technologies, Carlsbad, CA) + 5% Horse Serum (Life Technologies, Carlsbad, CA) + 20 ng/ml of Epidermal Growth Factor (EGF) (Peprotech, NJ) + 0.5 mg/ml of Hydrocortisone (Sigma–Aldrich, St. Louis, MO) + 100 ng/ml Cholera Toxin (Sigma–Aldrich, St. Louis, MO) + 10 μg/ml of Insulin (Sigma–Aldrich, St. Louis, MO) + 1% Pen/Strep (Life Technologies, Carlsbad, CA). AG11132 cells were cultured in MEGM™ Mammary Epithelial Cell Growth Medium (Lonza, Allendale, NJ).

2.2. Immunostaining

Human CXCR4 Phycoerythrin MAb (FAB170P) was purchased from R&D Systems (Minneapolis, MN). Cells were collected on glass slides or treated with a 0.05% trypsin/EDTA solution, rinsed twice with PBS, and then blocked with 1% bovine serum albumin (BSA) in PBS for 30 min in an ice bath. Cells were incubated with antibody for 1 h at RT. Cells were rinsed with 1% BSA in PBS three times. Confocal microscopy was performed on an LSM 710 Confocal Microscope (Zeiss, Germany). A BD LSRII Analyzer (BD Biosciences, CA) was used for flow cytometry analysis.

2.3. Surface density

The CXCR4 surface density was determined by flow cytometry using a calibration based on the Quantum™ Simply Cellular(R) anti-Mouse IgG microbeads (Bangs Laboratory, Inc., IN). The protocol used was as provided by the manufacturer. The number of molecules per μm^2 was calculated by dividing the total number of molecules by the average cell surface area.

2.4. Atomic force microscopy

AFM experiments were performed on an Asylum MFP-3D SA AFM (Asylum Research, CA), with silicon nitride, four sided pyramid tips (BL-TR400PB-35, Asylum Research, CA). The spring constant of the tips were calibrated every time by the Thermal Method, all tips used have a spring constant between 0.02 and 0.04 N/m. Cells were cultured in a 35 mm Petri dish. The AFM was performed in contact mode, with a trigger voltage of 0.5 V. The scan rate was 1 Hz, and the scan size was 10 μm by 10 μm, unless otherwise specified.

Tip functionalization has three steps; the first step is to introduce amine groups to the tip surface [6–10] by amino-functionalization with (3-Aminopropyl)triethoxysilane (APTES) vapors in the gas phase, using vapors of triethylamine as a catalyst. The second step is to covalently tether the NHS- end of the cross-linker acetal- Polyethylene glycol (PEG) -NHS to the amino terminated tips [11]. PEG chains with a length of 6–10 nm are considered optimal. The third step is the conversion of the Acetal-into an Aldehyde-by immersing the cantilever in 1% citric acid (in water). The antibody is then attached to the Aldehyde-end of the PEG linker in the presence of 1 M sodium cyanoborohydride (to convert the initially formed C=N bond into a stable C–N bond).

To measure the density of antibody on the AFM tip, the Neutravidin-Peroxidase [12] assay was used. The AFM tip was mimicked by a silicon nitride disc (3 mm of diameter, surface is 1.41×10^7 μm^2), which is the same material as the AFM tip but has a larger surface. The disc was functionalized using the same procedure as for the AFM tips, except using a biotin-PEG-NHS linker. The number of biotin groups was quantified by measuring the amount of labeled Neutraavidin bound to biotin. Reaction with peroxidase produces a brown color, which can be measured by UV-spectroscopy. The Extravidin-peroxidase stock solution from Sigma–Aldrich (St. Louis, MO) has an average protein concentration of 2 mg/mL (or 16.7 μM) and an average peroxidase/avidin ratio of 0.7. The stock solution was diluted by a factor of 2000, which yields 5×10^9 enzyme molecules/μL. A calibration curve was prepared with known amounts of biotin. The density of antibody on each tip was determined to be 1264 ± 357 molecule/μm^2.

A force–distance curve describing a single approach-retract cycle of the AFM tip is shown in Fig. 1, which is repeated during AFM mapping. The AFM tip is approaches the sample surface (A). The initial contact between the tip and the surface is mediated by attractive van der Waals forces (contact) that lead to an attraction of the tip toward the surface (B). Hence, the tip applies a constant and default force upon the surface that leads to sample indentation and cantilever deflection (C). Subsequently, the tip tries to retract from the surface (D). The unbinding force, between the sample and the AFM tip, hampers tip retraction. These unbinding forces can be taken directly from the force–distance curve (E). The tip withdraws and loses contact to the surface upon overcoming the unbinding forces (F).

The Young's modulus is determined by fitting B–C by the Hertz equation [13,14]. The quasi-static force F is related to the indentation depth δ:

$$F = \frac{E}{1-\nu^2}\frac{\tan\beta}{\sqrt{2}}\delta^2 \quad (1)$$

where β is the face angle, ν is Poisson's ratio of the material assumed here to be 0.5 (isotropic incompressible), and E is the Young's modulus.

2.5. Lipid raft delocalization

To disrupt lipid rafts, we added Methyl-β-cyclodextrin (MCD) (Sigma–Aldrich, St. Louis, MO) to cells, MCD is widely used as a cholesterol chelator, however cytotoxic effects may be observed above 5 mM. In this work, three cell lines MDA-MB-231, MCF-7 and MCF 10A were treated with 5 mM of MCD for 1 h at 37 °C after activation with IL-1α for 6 h then washed twice with PBS and resuspended in 1.5 ml of warm cell culture medium in a 35 mm Petri dish.

2.6. Hydrogel preparation

Gelatin hydrogels were prepared by dissolving gelatin powder (G-Biosciences, MO) under stirring in 40°C PBS for 1 h. One milliliter of gelatin solution (10%w/v) was transferred into a 35 mm Petri dish for a thickness of 1 mm. After 1 h of water evaporation at RT, the gels were crosslinked by adding 1 ml of 0.5% w/w glutaraldehyde solution in PBS for 1 h at RT. The crosslinked samples were washed with distilled water, air dried at RT, and sterilized by UV light for 30 min. To improve cell adhesion, the gelatin gel surface was treated with 1 ml of 30 μg/mL fibronectin (Corning, NY) in PBS for 1 h. The fibronectin solution was aspirated and the gelatin gel surface was washed twice in PBS before cells were seeded.

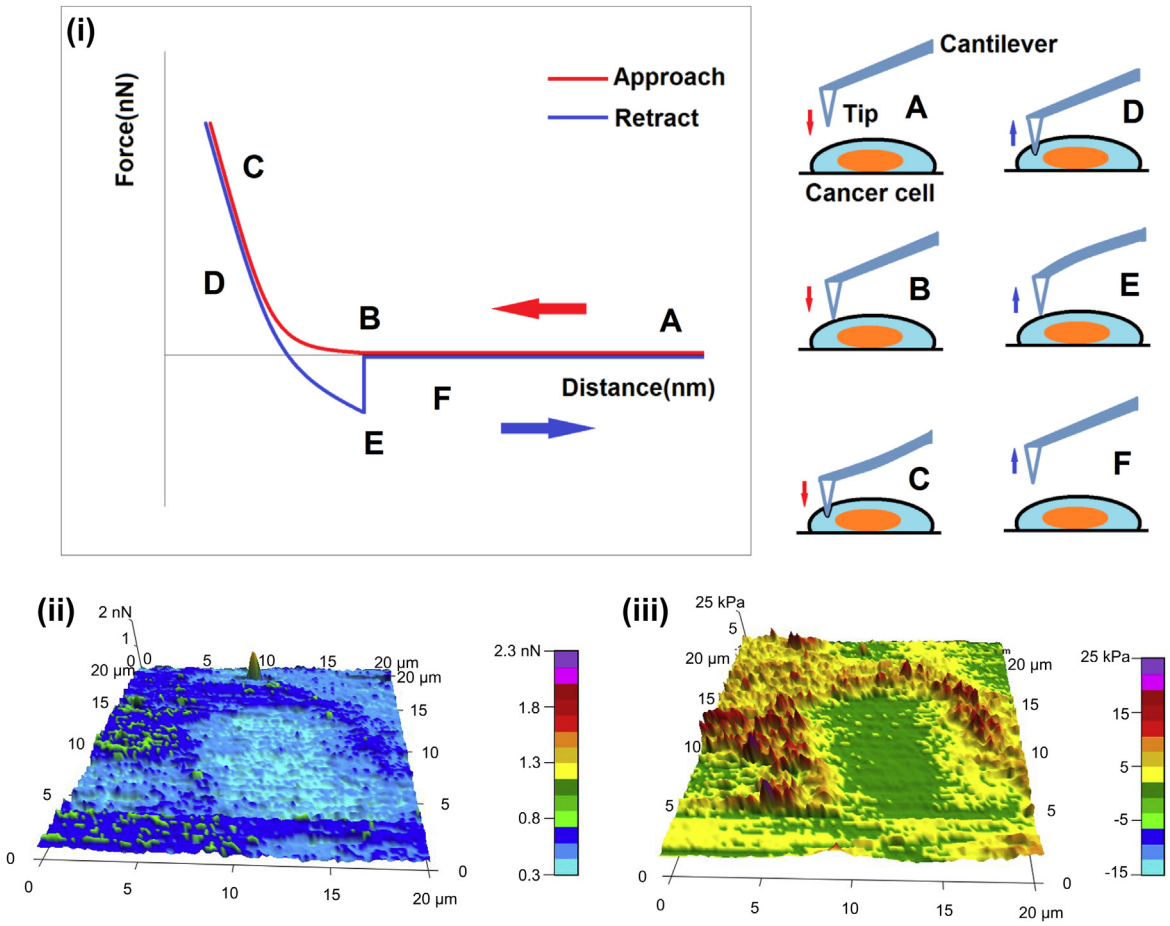

Fig. 1. AFM force spectroscopy of live cells. (i) AFM measurement for rheology and unbinding force data. (ii) Young's modulus map for MCF-10A cells detected from B to C (iii) Unbinding force map for MCF-10A cells detected from E to F.

3. Results and discussion

3.1. Young's modulus

We measured the Young's modulus of two nonneoplastic, human mammary epithelial cell lines MCF-10A and AG11132, and four breast cancer cell lines of various ER/PR/HER2 status (Fig. 2). Metastatic cancer cells with low Young's modulus relative to control cells are hypothesized to facilitate migration out of the primary tumor into circulation [16]. Our results show that breast cancer cells had lower Young's modulus between 1 and 3 kPa than control MCF-10A cells (6 kPa) and AG11132 cells (6 kPa).

The AFM measurements probed local stiffness across a 10 μm by 10 μm square area. This resulted in histograms of the Young's modulus for each cell type. Substantial heterogeneity across the cell was observed. The overall distribution was wide for MCF-10A cells relative to the narrow distribution in the breast cancer cells. Heterogeneity, at the micron scale, and a high Young's modulus were characteristic of a control cell phenotype. Breast cancer cells were more homogenous and exhibited lower average Young's modulus relative to control cells.

Several techniques are used to measure the Young's modulus of cells, including micropipette aspiration [17], two microplates method [18], optical tweezers [19], magnetic twisting cytometry [20], and rotational microrheology [21]. These techniques report an average Young's modulus within a similar range as our results; they assume that the Young's modulus is uniform over the entire cell. Breast cancer cells are known to have a lower Young's modulus relative to control cells: Li et al. found the Young's modulus of MCF-7 was 0.6 kPa in comparison to MCF-10A (1.2 kPa) [22]. Nikkhah et al. found MDA-MB-231 cells and MCF-10A cells to have a Young's modulus of 0.4 ± 0.2 kPa and 0.7 ± 0.5 kPa, respectively [23]. The homogenous and elastic nature of breast cancer cells suggests structural differences, which impart different mechanical properties.

The ramp size and the ramp velocity may be responsible for differences in the magnitude of the Young's modulus; for MCF-7 cells, it can increase from 4.5 ± 2.0 kPa to 25 ± 10 kPa when the ramp size decreases from 2 μm to 500 nm and the ramp velocity drops from 2 μm/s to 500 nm/s [24]. The ramp size and velocity used here were 4 μm and 500 nm/s, and used consistently throughout experiments.

3.2. CXCR4 density

Gene expression analysis and histology have shown increased CXCR4 presentation amongst metastatic breast cancer tumors and cell lines [4]. Consequently, therapeutics that bind CXCR4 reduced metastasis in animal models [25]. The factors that influence CXCR4 receptor binding and potentially regulate the therapeutic effect

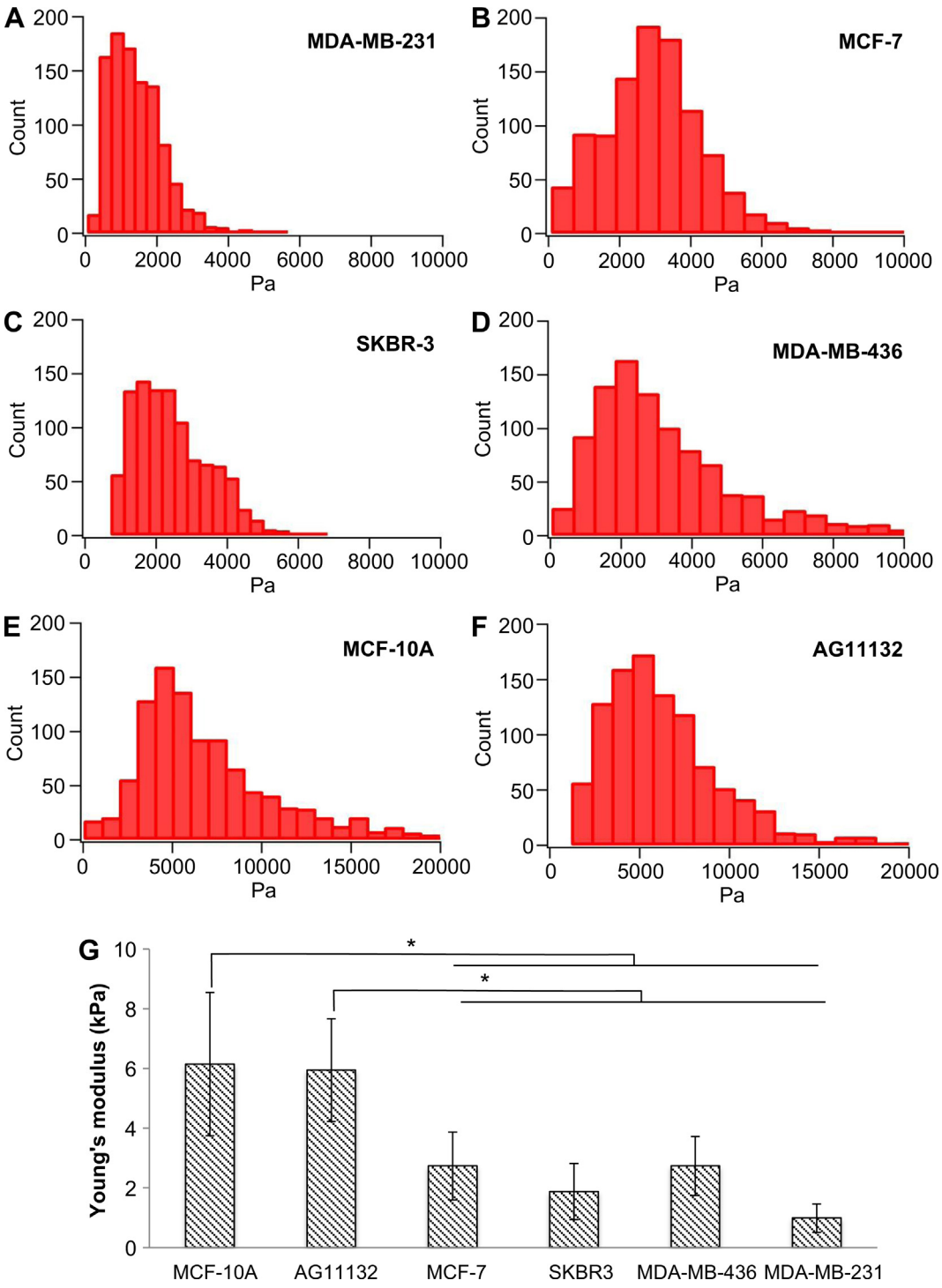

Fig. 2. Histogram of the Young's modulus of breast cancer cells (A–D) in comparison with non-malignant epithelial cell MCF10A (E) and AG11132 (F). The average Young's modulus (n = 5) (G). Error is calculated using a Two sample Student's t test, where an * denotes a confidence interval of 95%.

include the average surface density, the spatial distribution, and the unbinding force of CXCR4.

We measured the surface density of CXCR4 in four breast cancer cell lines by flow cytometry (Table 1). The average CXCR4 protein density ranged from 40.7 to 143.5 molecules/μm^2. The nonneoplastic cell lines MCF-10A and AG1132 exhibited 24.2 ± 6.3 and 16.4 ± 4.7 molecules/μm^2, respectively, demonstrating that CXCR4 is more highly expressed in breast cancer cells relative to the nonneoplastic cell line.

3.3. CXCR4 unbinding force

The spatial organization of CXCR4 and its unbinding force were probed by a tip covalently conjugated with anti-CXCR4 (Fig. 3). The spatial distribution of MCF-10A and AG11132 showed a random, but uniformly dispersed distribution of unbinding forces across the cell membrane. In contrast, all four breast cancer cell lines exhibited heterogeneous patterns of high unbinding forces.

Table 1
Characterization of breast cancer cell lines and two non-neoplastic, mammary cell line (MCF-10A and AG11132). Error is calculated as the standard deviation from the mean.

Cell line	ER	PR	HER2	Receptor density (molecules/μm2)
MDA-MB-231	–	–	–	89.1 ± 30.1
MDA-MB-436	–	–	–	143.5 ± 22.9
MCF-7	+	+	–	62.8 ± 18.7
SKBR-3	–	–	++	40.7 ± 6.5
MCF-10A	–	–	–	24.2 ± 6.3
AG11132	–	–	–	16.4 ± 4.7

The average unbinding force for breast cancer cells ranged between 149 and 257 pN. The control cells MCF-10A and AG11132 exhibited unbinding forces of 188 ± 40 pN and 208 ± 32 pN, respectively. The magnitude of the unbinding force is similar in magnitude to other ligand-receptor pairs (e.g. sialyl Lewis X (sLeX)–P-selectin interaction [7] streptavidin/biotin binding [26]). No statistical difference was found between the different cell types. Surprisingly, we did not see a correlation between the CXCR4 surface density and the average unbinding force. This suggests that the organization of the CXCR4 receptors may be driving differences in binding.

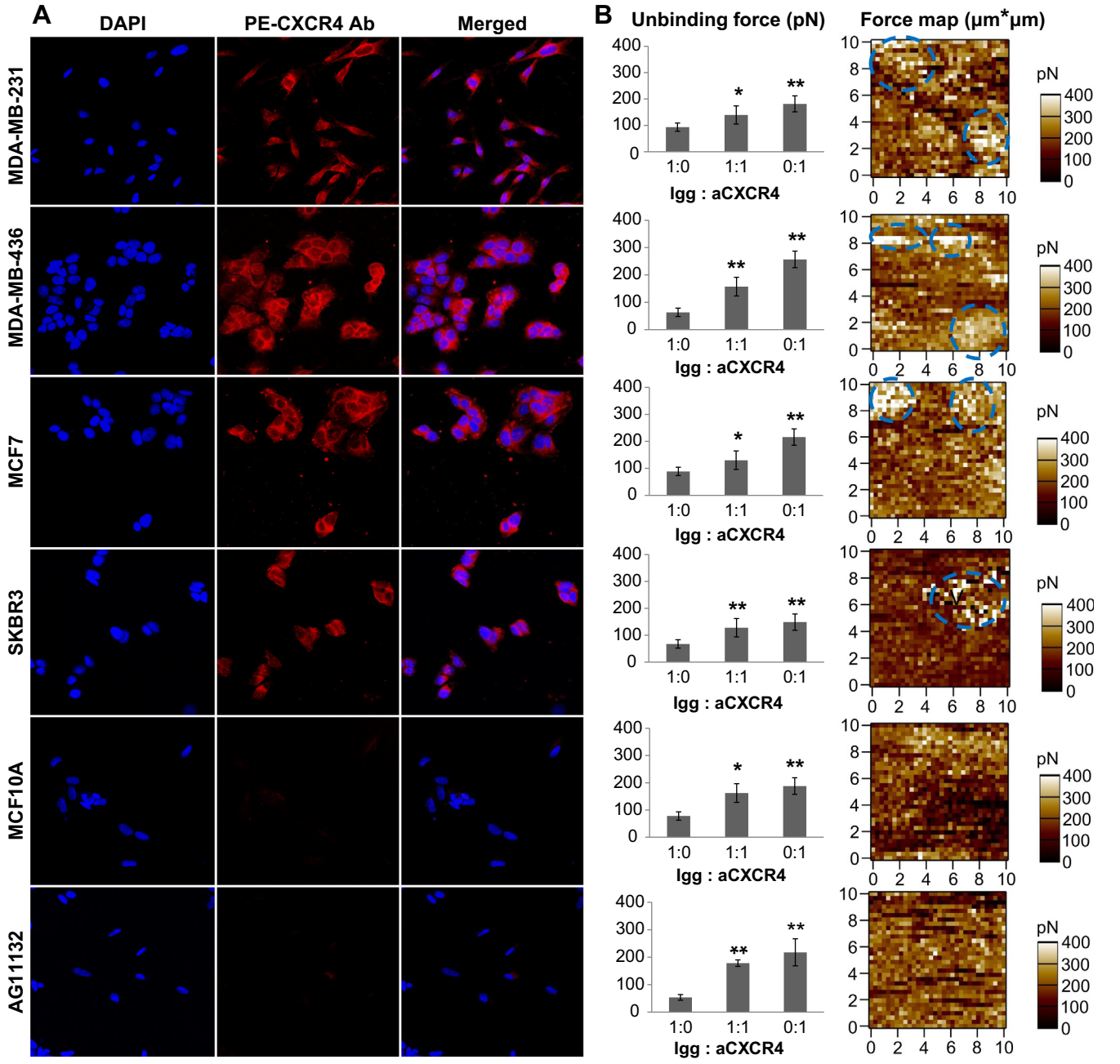

Fig. 3. Identification of CXCR4 as a biomarker. (A) Fluorescent micrographs of MDA-MB-231, MDA-MB-436, MCF7, SKBR3, MCF10A and AG11132 stained with an anti-human CXCR4 PE-conjugated antibody (red). DAPI (blue) was used to stain the cell nuclei. (B) The unbinding force of MDA-MB-231, MDA-MB-436, MCF7, SKBR3, MCF10A and AG11132. Error is calculated using a two sample Student's t test, where * and ** denote a confidence interval of 95% and 99%, respectively. The scale bar is 20 μm. (For interpretation of the references to colour in this figure legend, the reader is referred to the web version of this article.)

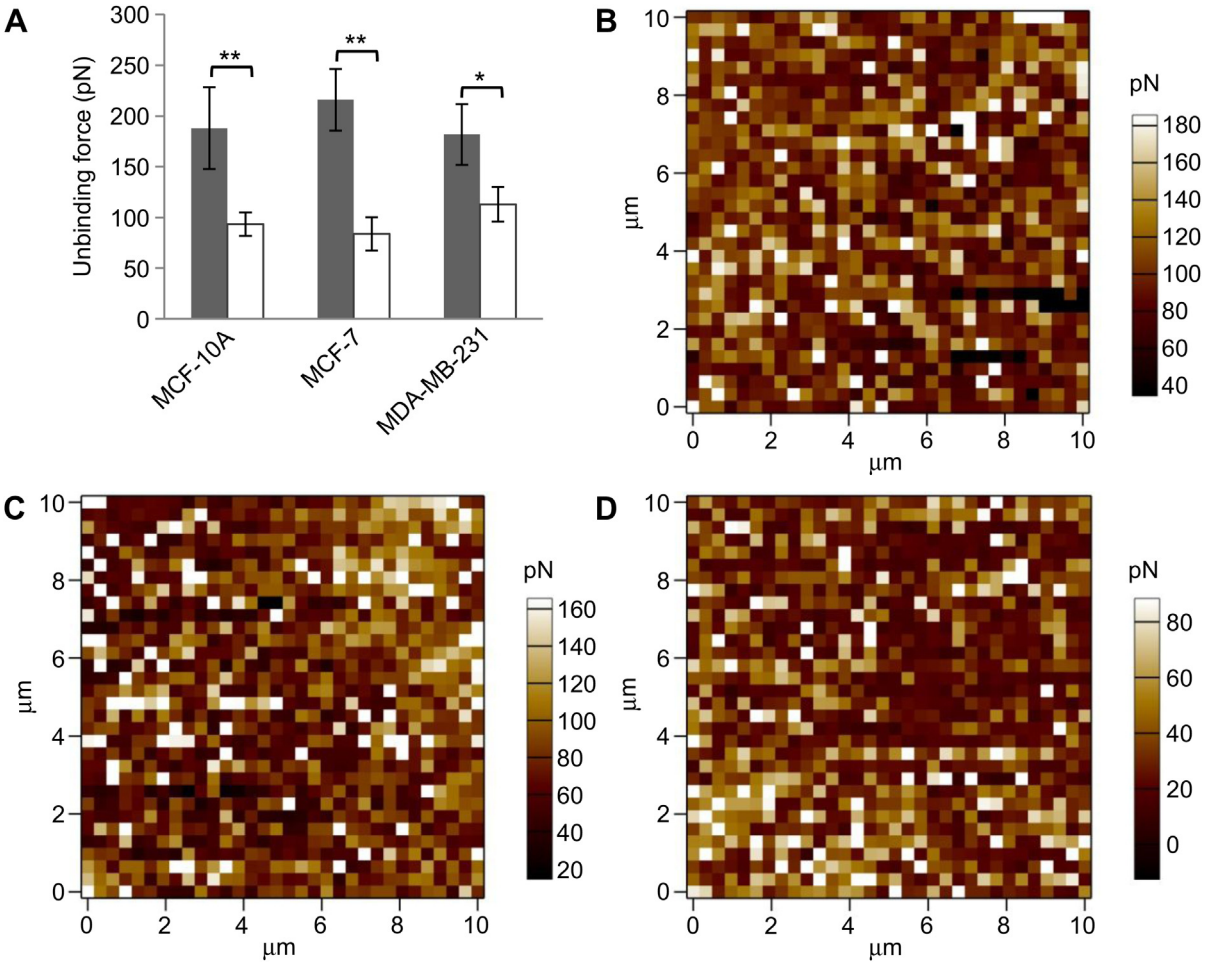

Fig. 4. Comparison of the unbinding force with (white) or without (black) methyl-β-cyclodextrin (MCD). (A) The average unbinding force measured in two breast cancer cells lines relative to MCF-10A. (B–D) AFM maps of CXCR4 binding on breast cancer cells incubated with MCD. Error is calculated using a Two sample Student's t test, where a * and ** denotes a confidence interval of 95% and 99%, respectively.

The effect of the density of anti-CXCR4 molecules on the AFM tip was probed by the addition of equal concentrations of both nonspecific IgG and anti-CXCR4. The reduction in anti-CXCR4 density resulted in a reduction in the average unbinding force. There was no statistical difference in the unbinding force for MCF-10A and AG11132 cells when the AFM tip anti-CXCR4 surface density was halved (Fig. 3, 1:1 vs. 0:1). In contrast, the MCF-7, MDA-MB-436, and MDA-MB-231 cells exhibited a density-dependent unbinding force. This confirms that multiple anti-CXCR4 molecules are binding CXCR4 receptors on the cell surface.

3.4. CXCR4 organization

For optimal signaling, CXCR4 must be embedded in membrane lipid rafts that are rich in cholesterol [27–29]. Cholesterol dependent ligand-receptor binding has been reported [30]. Cholesterol is involved in membrane stiffening by reducing lipid packing [31] and in lipid raft formation [32]. The impact of CXCR4 colocalization on the unbinding force was confirmed by the addition of the cholesterol chelator MCD. MCD blocks the association between CXCR4 and other receptors, e.g., CD45 [33], and disrupts lipid raft organization. It has been reported that the cancer cell lines (MCF-7, MDA-MB-231) have higher cholesterol levels than control cell lines (MCF-10A) [34]. After 5 mM of MCD treatment, the cellular cholesterol level is reduced by 90% compared to untreated cells [35]. Our results show that the addition of MCD causes changes in the spatial distribution of the unbinding force maps of MCF-7 and MDA-MB-231, from heterogeneous to homogenous (Fig. 4). The average unbinding force decreased by 2.0, 2.6, and 1.6-fold for MCF-10A, MCF-7, and MDA-MB-231, respectively. The significant reduction in the unbinding force upon addition of MCD confirms that the organization of CXCR4 within lipid rafts is an important aspect of ligand-receptor interactions.

3.5. Matrix stiffness

Matrix stiffness is regarded as an important characteristic governing cell adhesion, migration, and gene regulation [36]. Cells were plated on gelatin to determine the impact of surface stiffness on CXCR4 organization. The Young's modulus of gelatin was measured to be 350 ± 40 kPa, approximately four orders of magnitude softer than tissue culture plastic (TCP) [37]. Gelatin is a derivative of collagen, which is a major component of the extracellular matrix (ECM). It has been used to synthesize hydrogels and scaffolds for tissue engineering due to its biocompatibility, biodegradability, cell adhesion characteristics, and mechanical properties [38]. In breast cancer, collagen deposition and alignment correlates with poor prognosis [39].

Here, we observed that the unbinding force of breast cancer cells cultured on gelatin were significantly higher than unbinding

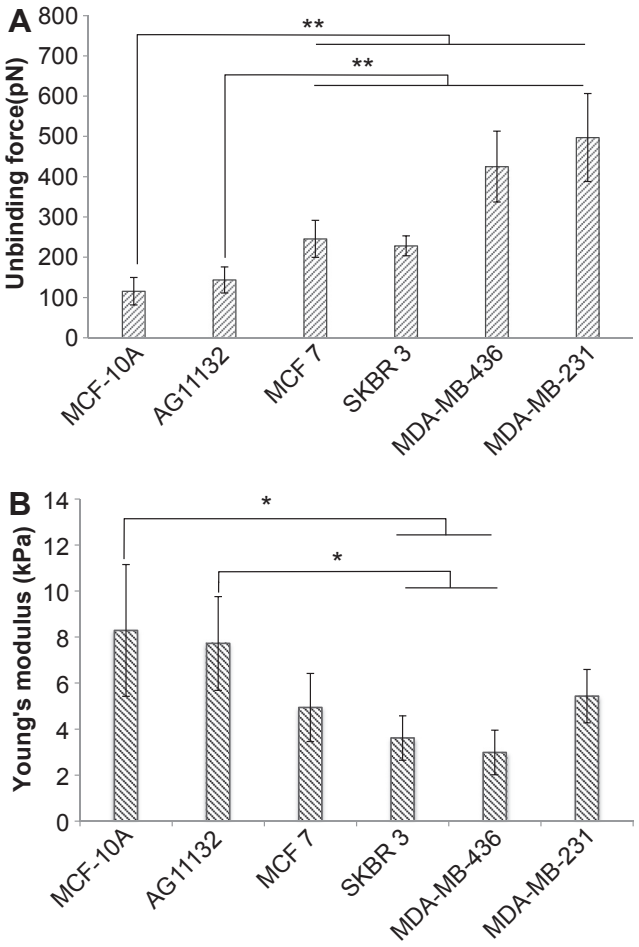

Fig. 5. The average unbinding force (A) and Young's modulus (B) of four breast cancer cells in comparison with two normal epithelial phenotype (MCF-10A and AG11132) on a gelatin gel. Error is calculated using a Two sample Student's t test, where a * and ** denotes a confidence interval of 95% and 99%, respectively.

forces of cells cultured on TCP (Fig. 5). TNBC cells, MDA-MB-231 and MDA-MB-436, exhibited more than 3-fold higher unbinding forces relative to control cells on gelatin. MCF-7 and SKBR3 cells were almost 2-fold higher than control cells on gelatin. In contrast, the unbinding force of non-TNBC cells were comparable. The CXCR4 density accurately predicts the unbinding force when cells are plated on gelatin.

The Young's modulus of the cells tested did not change when plated on gelatin with the exception of MDA-MB-231. MDA-MB-231 cells increased in stiffness when plated on gelatin; their Young's modulus was still significantly lower than MCF-10A and AG11132 cells.

The measured unbinding force includes the intermolecular force governing the ligand/receptor interaction along with the binding energies that contribute to the stabilization of the ligand/receptor complex. These additional forces may also be affected by local organization which may be inferred indirectly from thermodynamic and kinetic approaches [40].

Knowledge of receptor-ligand unbinding forces may lead to the development of a rigorous approach to identify receptors for targeted drug delivery. Stronger binding to cancer cells relative to a control may yield more precise and efficient cancer-targeting due to improved discrimination between breast cancer cells and non-neoplastic cells. Improved accumulation of chemotherapeutics and diagnostic molecules at sites of interest may reduce adverse side effects and improve tumor detection. Current methods to identify receptors to target cancer cells rely on overexpression and do not account for receptor-ligand interactions. Both metrics could be used as a screening tool for preclinical and clinical investigations.

4. Conclusion

Understanding CXCR4 binding mechanics on live breast cancer cells may be an important step to understanding ligand-receptor interactions that govern breast cancer migration. Breast cancer diagnostics and therapeutics may rely on the design of synthetic surfaces that interact specifically with biological membranes. A higher density of CXCR4 on breast cancer cells relative to control cells assigns a higher probability to being a therapeutic target, but may only be one factor. Here, we show that CXCR4 density, organization, cholesterol content, and matrix stiffness all affect the unbinding force of CXCR4. The receptor density did not correlate with unbinding forces when cultured on TCP; however, TNBC cells – having the highest CXCR4 densities - showed 3-fold higher unbinding forces relative to control when cultured on gelatin. Therefore, unbinding force measurements on cells cultured on gelatin may be useful in drug delivery vehicle design for preferential binding and uptake.

Acknowledgments

The authors would like to acknowledge funding from the NIH (NCI DP2 CA174495-01).

References

[1] Siegel R, Ma J, Zou Z, Jemal A. Cancer statistics, 2014. CA: A Cancer J Clin 2014;64:9–29.
[2] Howlader N, Noone AM, Krapcho M, Garshell J, Miller D, Altekruse SF, et al. SEER Cancer statistics review, 1975–2011. National Cancer Institute; 2013.
[3] Mukherjee D, Zhao J. The role of chemokine receptor CXCR4 in breast cancer metastasis. Am J Cancer Res 2013;3:46–57.
[4] Müller A, Homey B, Soto H, Ge N, Catron D, Buchanan ME, et al. Involvement of chemokine receptors in breast cancer metastasis. Nature 2001;410:50–6.
[5] Binnig G, Quate CF. Atomic force microscope. Phys Rev Lett 1986;56:930–3.
[6] Girish CM, Binulal NS, Anitha VC, Nair S, Mony U, Prasanth R. Atomic force microscopic study of folate receptors in live cells with functionalized tips. Appl Phys Lett 2009;95:223703.
[7] Hinterdorfer P, Dufrêne YF. Detection and localization of single molecular recognition events using atomic force microscopy. Nat Methods 2006;3:347–55.
[8] Ebner A, Wildling L, Kamruzzahan ASM, Rankl C, Wruss J, Hahn CD, et al. A new, simple method for linking of antibodies to atomic force microscopy tips. Bioconjug Chem 2007;18:1176–84.
[9] Ebner A, Hinterdorfer P, Gruber HJ. Comparison of different amino-functionalization strategies for attachment of single antibodies to AFM cantilevers. Ultramicroscopy 2007;107:922–7.
[10] Chtcheglova LA, Hinterdorfer P. Functional AFM imaging of cellular membranes using functionalized tips. Methods Mol Biol 2013;950:359–71.
[11] Wildling L, Unterauer B, Zhu R, Rupprecht A, Haselgrübler T, Rankl C, et al. Linking of sensor molecules with amino groups to amino-functionalized AFM tips. Bioconjugate Chem 2011;22:1239–48.
[12] Riener CK, Stroh CM, Ebner A, Klampfl C, Gall AA, Romanin C, et al. Simple test system for single molecule recognition force microscopy. Anal Chim Acta 2003;479:59–75.
[13] Chu Y-S, Dufour S, Thiery JP, Perez E, Pincet F. Johnson-Kendall-Roberts theory applied to living cells. Phys Rev Lett 2005;94:028102.
[14] Guevorkian K, Colbert M-J, Durth M, Dufour S, Brochard-Wyart F. Aspiration of biological viscoelastic drops. Phys Rev Lett 2010;104:218101.
[16] Suresh S. Biomechanics and biophysics of cancer cells. Acta Mater 2007;55:3989–4014.
[17] Hochmuth RM. Micropipette aspiration of living cells. J Biomech 2000;33:15–22.
[18] Caille N, Thoumine O, Tardy Y, Meister J-J. Contribution of the nucleus to the mechanical properties of endothelial cells. J Biomechanics 2002;35:177–87.
[19] Zhang H, Liu K-K. Optical tweezers for single cells. J R Soc Interface 2008;5:671–90.

[20] Na S, Wang N. Application of fluorescence resonance energy transfer and magnetic twisting cytometry to quantify mechanochemical signaling activities in a living cell. Sci Signal 2008;1:pl1.
[21] Wilhelm C, Gazeau F, Bacri J-C. Rotational magnetic endosome microrheology: Viscoelastic architecture inside living cells. Phys Rev E 2003;67:061908.
[22] Li QS, Lee GYH, Ong CN, Lim CT. AFM indentation study of breast cancer cells. Biochem Biophysical Res Commun 2008;374:609–13.
[23] Nikkhah M, Strobl JS, Schmelz EM, Agah M. Evaluation of the influence of growth medium composition on cell elasticity. J Biomechanics 2011;44:762–6.
[24] Zhang W, Kai K, Choi DS, Iwamoto T, Nguyen YH, Wong H, et al. Microfluidics separation reveals the stem-cell-like deformability of tumor-initiating cells. Proc Natl Acad Sci 2012;109:18707–12.
[25] Liang Z, Wu T, Lou H, Yu X, Taichman RS, Lau SK, et al. Inhibition of breast cancer metastasis by selective synthetic polypeptide against CXCR4. Cancer Res 2004;64:4302–8.
[26] Yuan C, Chen A, Kolb P, Moy VT. Energy landscape of Streptavidin–Biotin complexes measured by atomic force microscopy †. Biochemistry 2000;39:10219–23.
[27] Nguyen DH, Taub D. CXCR4 function requires membrane cholesterol: implications for HIV infection. J Immunol 2002;168:4121–6.
[28] Wysoczynski M. Incorporation of CXCR4 into membrane lipid rafts primes homing-related responses of hematopoietic stem/progenitor cells to an SDF-1 gradient. Blood 2005;105:40–8.
[29] Schabath H. CD24 affects CXCR4 function in pre-B lymphocytes and breast carcinoma cells. J Cell Sci 2006;119:314–25.
[30] Burger K, Gimpl G, Fahrenholz F. Regulation of receptor function by cholesterol. Cell Mol Life Sci 2000;57:1577–92.
[31] Birukov KG. Loose cholesterol, get stiff! focus on "oxLDL-induced decrease in lipid order of membrane domains is inversely correlated with endothelial stiffness and network formation." AJP: Cell Physiol 2010;299:C211–2.
[32] Silvius J. Role of cholesterol in lipid raft formation: lessons from lipid model systems. Biochimica Biophysica Acta (BBA) – Biomembr 2003;1610:174–83.
[33] Fernandis AZ, Cherla RP, Ganju RK. Differential regulation of CXCR4-mediated T-cell chemotaxis and mitogen-activated protein kinase activation by the membrane tyrosine phosphatase, CD45. J Biol Chem 2003;278:9536–43.
[34] Li YC, Park MJ, Ye S-K, Kim C-W, Kim Y-N. Elevated levels of cholesterol-rich lipid rafts in Cancer cells are correlated with apoptosis sensitivity induced by cholesterol-depleting agents. Am J Pathol 2006;168:1107–18.
[35] Danthi P, Chow M. Cholesterol removal by methyl-beta-cyclodextrin inhibits poliovirus entry. J Virol 2004;78:33–41.
[36] Engler AJ, Sen S, Sweeney HL. Discher DE.Matrix elasticity directs stem cell lineage specification. Cell 2006;126:677–89.
[37] Wells RG. The role of matrix stiffness in regulating cell behavior. Hepatology 2008;47:1394–400.
[38] Conklin MW, Eickhoff JC, Riching KM, Pehlke CA, Eliceiri KW, Provenzano PP, et al. Aligned collagen is a prognostic signature for survival in human breast carcinoma. Am J Pathol 2011;178:1221–32.
[39] Drury JL, Mooney DJ. Hydrogels for tissue engineering: scaffold design variables and applications. Biomaterials 2003;24:4337–51.
[40] Lee C-K, Wang Y-M, Huang L-S, Lin S. Atomic force microscopy: determination of unbinding force, off rate and energy barrier for protein-ligand interaction. Micron 2007;38:446–61.